Accounting for the influence of the free surface on the vibration response of underground railway tunnels: a new iterative method

T. L. Edirisinghe [1]**, J. P. Talbot** [1]**, M. F. M. Hussein** [2]

[1] University of Cambridge, Department of Engineering
Cambridge, CB2 1PZ, United Kingdom
e-mail: **tle25@cam.ac.uk**

[2] Qatar University, Department of Civil and Architectural Engineering, College of Engineering
P.O. Box 2713, Doha, Qatar

Abstract

This paper presents a new method for calculating the ground-borne vibration from shallow underground railways. The method is based on an iterative wave-scattering approach, which decouples the problem into two sub-systems: (1) a tunnel embedded in a full-space and (2) a half-space domain for the soil alone. The Pipe-in-Pipe (PiP) model is first used to find the soil response remote from the tunnel, in the absence of a free surface. The reflected wave-field approaching the soil-tunnel interface from the free surface is then computed using a Boundary-Element Method (BEM) model, before applying this as an external load on the tunnel wall to calculate the revised response. The process is repeated for multiple iterations until convergence is achieved. To the authors' knowledge, this is the first time that an iterative approach has been applied to an elastodynamic problem. The results from this iterative PiP-BEM model are compared with those of a coupled Finite-Element-Boundary-Element Method (FEM-BEM) model and found to agree well over the frequency range typically associated with ground-borne vibration.

1   Introduction

Vibration generated by the passage of underground trains can have a significant environmental impact on nearby structures. Vibration is generated at the wheel-rail interface and this can propagate through the soil into nearby buildings, where it may disturb occupants and lead to the malfunctioning of vibration-sensitive equipment. This has generated research interest in numerically modelling ground-borne vibration problems on account of increasing public sensitivity to noise and vibration and the introduction of new underground lines in urban areas.

One well-regarded numerical tool is the Pipe-in-Pipe (PiP) model [1], which is a computationally efficient software package for predicting the soil response around a railway tunnel. In the model, the tunnel invert can be excited either by a time-harmonic point force or by a train-track system, such as when a wheel-rail roughness is applied at axle masses on a floating-slab track (FST) [2]. The standard PiP model is derived by assuming the tunnel is embedded in a full-space [3] and then appropriate Green's functions are used with the fictitious-force method to account for when the tunnel is, instead, embedded in either a homogeneous [4] or a multi-layered [5] half-space. Multiple studies have concluded that there is good agreement between the PiP model and more rigorous Finite-Element-Boundary-Element Method (FEM-BEM) models [6] over the frequency range of 1–80 Hz, which is typically of interest for the perception of ground-borne vibration.

The fictitious-force method assumes that the near-field around the tunnel is not influenced by the existence of the free surface, i.e. the displacement at the soil-tunnel interface is the same whether or not there is a free surface. This assumption is valid when the distance between the tunnel crown and free surface is greater than the longest wavelength in the soil. However, when the tunnel is closer to the free surface, the response between the tunnel and free surface becomes coupled and the influence of the free surface cannot be neglected. Hussein et al. [7] compare the half-space PiP model against the 2.5D coupled FEM-BEM model of François et al. [8] for a tunnel embedded at different depths, when a point force is applied at the tunnel invert. At some frequencies, there are deviations in excess of 15 dB between the two models for the free-surface displacements generated by shallow tunnels.

The objective of this paper is to account more fully for the presence of the free surface in the half-space PiP model by proposing an iterative wave-scattering approach, and to assess the accuracy of this approach for realistic cases. The paper is organised as follows. Section 2 outlines the three distinct calculation steps in the proposed method. Section 3 presents a numerical study in which the results are compared against those from the equivalent 2.5D coupled FEM-BEM model [8]. Finally, Section 4 presents the conclusions and outlines some further work.

2 Method

In principle, an iterative wave-scattering approach can be used to dynamically couple two isolated sub-systems by accounting for the waves that propagate back-and-forth between them. The isolated sub-systems in this problem represent: (1) a tunnel embedded in a full-space and (2) a half-space domain for the soil. Iterative approaches have been applied to analyse wave-scattering problems involving elastic waves [9], [10], but, to the authors' knowledge, they have not been applied to an elastodynamic problem involving soil-embedded structures.

(a) Full-space PiP model   **(b)** Fictitious-force method   **(c)** BEM model
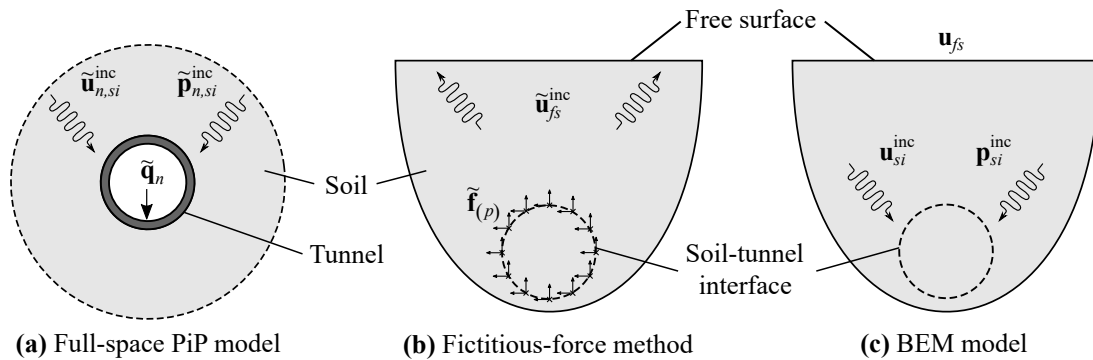
Figure 1: Implementation of the proposed iterative wave-scattering approach for a tunnel-soil system.

The method presented here consists of three main steps, as summarised in Fig. 1. In the first step (Fig. 1(a)), the full-space PiP model is used to calculate the response of the tunnel sub-system due to the directly applied excitation. In the second step (Fig. 1(b)), the fictitious-force method is applied to the soil sub-system to find the displacement field at the free surface. In the third step (Fig. 1(c)), the Boundary-Element Method (BEM) is used to calculate the wave-fields reflected from the free surface towards the soil-tunnel interface (evaluated at internal points in the soil domain). The reflected waves from the free surface are then applied to the tunnel sub-system used in the first step to revise the response at the tunnel. Thus, the three steps are repeated as an iterative process. During each iteration, the tunnel and soil sub-systems are weakly coupled together but, with multiple iterations, the combined response converges towards the fully coupled response, when the presence of the free surface is fully accounted for. All the equations given in this section are numerically implemented using the technical computing software, MATLAB [11].

An important concept of the iterative approach is that a field variable $\mathbf{u}$ at an interface can be expressed as the linear superposition of an incident field $\mathbf{u}^{\text{inc}}$ that propagates towards the interface and a scattered field $\mathbf{u}^{\text{sca}}$ formed by the wave interaction at the interface, such that $\mathbf{u} = \mathbf{u}^{\text{inc}} + \mathbf{u}^{\text{sca}}$. This is adopted in the following subsections, which outline each of the three steps.

2.1 Step 1: The iterative PiP model for a full-space

In the first calculation step, the full-space PiP model is used to calculate the response at the soil-tunnel interface due to a vertical, time-harmonic point force F_0 applied at the tunnel invert and, in subsequent iterations, incident displacement $\widetilde{\mathbf{u}}_{si}^{\text{inc}}$ and traction $\widetilde{\mathbf{p}}_{si}^{\text{inc}}$ fields at the outer tunnel wall, as illustrated in Fig. 2. The PiP model is based on a Fourier transformation from the time domain t to the frequency domain ω, and from the space domain x along the tunnel's longitudinal axis to the wavenumber domain ξ. Moreover, a Fourier series expansion is employed in the circumferential direction θ to evaluate the response in terms of n discrete circumferential ring-modes. Only a finite number of modes is necessary to achieve convergence in the response; it is found that $n = 10$ achieves this.

The tunnel is modelled as an infinite, thick-walled shell with outer radius r_{to} and inner radius r_{ti}, and the soil is modelled as an infinite, cylindrical cavity with infinite outer radius $r_{so} \to \infty$ and inner radius $r_{si} = r_{to}$. The three-dimensional response of the tunnel and full-space are described by their radial, circumferential and longitudinal components in the cylindrical coordinate system (r, θ, x). Thus, the displacement and traction fields in the soil-tunnel system are expressed as $\mathbf{u}(r, \theta, x, \omega) = \{u_r, u_\theta, u_x\}^{\text{T}}$ and $\mathbf{p}(r, \theta, x, \omega) = \{\sigma_{rr}, \sigma_{r\theta}, \sigma_{rx}\}^{\text{T}}$, respectively, where T denotes the vector transpose.
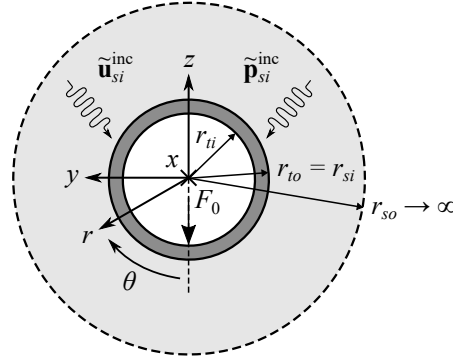

Figure 2: A tunnel embedded in a full-space.

By implementing the inverse Fourier transform and the Fourier series expansion, it is straightforward to show that the point force F_0 at the tunnel invert can be expressed as the traction field:

$$\mathbf{q}(r, \theta, x, \omega) = \begin{Bmatrix} q_r \\ q_\theta \\ q_x \end{Bmatrix} = \frac{1}{2\pi} \int_{-\infty}^{\infty} \sum_{n=0}^{\infty} \begin{Bmatrix} \widetilde{q}_{rn} \cos n\theta \\ \widetilde{q}_{\theta n} \sin n\theta \\ \widetilde{q}_{xn} \cos n\theta \end{Bmatrix} \cdot e^{i\xi x} d\xi \,, \tag{1}$$

where the traction field components $\widetilde{\mathbf{q}}_n = \{\widetilde{q}_{rn}, \widetilde{q}_{\theta n}, \widetilde{q}_{xn}\}^{\text{T}}$ in the modal-wavenumber-frequency (n, ξ, ω)-domain are

$$\widetilde{q}_{rn}(n, \xi, \omega) = \begin{cases} \dfrac{F_0}{2\pi r_{ti}} & \text{for } n = 0 \,, \\[2mm] \dfrac{F_0}{\pi r_{ti}} & \text{for } n \geq 1 \,, \end{cases} \tag{2}$$

$$\widetilde{q}_{\theta n}(n, \xi, \omega) = \widetilde{q}_{xn}(n, \xi, \omega) = 0 \quad \text{for all } n \,.$$

Forrest and Hunt [12] employ wave potentials to derive the solution for elastic wave propagation in the tunnel and full-space, and describe the motion at the tunnel inner and outer walls as the following matrix equations:

$$\widetilde{\mathbf{u}}_{n,ti}(n,\xi,\omega) = \left.\widetilde{\mathbf{U}}\right|_{r=r_{ti}} \widetilde{\mathbf{c}}, \tag{3}$$

$$\widetilde{\mathbf{p}}_{n,ti}(n,\xi,\omega) = \left.\widetilde{\mathbf{T}}_r\right|_{r=r_{ti}} \widetilde{\mathbf{c}}, \tag{4}$$

$$\widetilde{\mathbf{u}}_{n,to}(n,\xi,\omega) = \left.\widetilde{\mathbf{U}}\right|_{r=r_{to}} \widetilde{\mathbf{c}}, \tag{5}$$

$$-\widetilde{\mathbf{p}}_{n,to}(n,\xi,\omega) = \left.\widetilde{\mathbf{T}}_r\right|_{r=r_{to}} \widetilde{\mathbf{c}}, \tag{6}$$

where the 6×1 vector $\widetilde{\mathbf{c}}$ denotes the equation coefficients for the motion of a thick-walled shell, and the 3×6 matrices $\widetilde{\mathbf{U}}(r,n,\xi,\omega)$ and $\widetilde{\mathbf{T}}_r(r,n,\xi,\omega)$ are given in closed form by Forrest and Hunt [12].

The scattered-fields at the soil-tunnel interface, due to the incident displacement $\widetilde{\mathbf{u}}_{n,si}^{\mathrm{inc}}$ and traction $\widetilde{\mathbf{p}}_{n,si}^{\mathrm{inc}}$ fields, can be expressed as the following matrix equations:

$$\widetilde{\mathbf{u}}_{n,si} - \widetilde{\mathbf{u}}_{n,si}^{\mathrm{inc}} = \left.\widetilde{\mathbf{U}}_m\right|_{r=r_{si}} \widetilde{\mathbf{b}}, \tag{7}$$

$$\widetilde{\mathbf{p}}_{n,si} - \widetilde{\mathbf{p}}_{n,si}^{\mathrm{inc}} = \left.\widetilde{\mathbf{T}}_m\right|_{r=r_{si}} \widetilde{\mathbf{b}}, \tag{8}$$

where the 3×1 vector $\widetilde{\mathbf{b}}$ denotes the equation coefficients for the motion of a cylindrical cavity, and the 3×3 matrices $\widetilde{\mathbf{U}}_m(r,n,\xi,\omega)$ and $\widetilde{\mathbf{T}}_m(r,n,\xi,\omega)$ contain the second, fourth and sixth columns of $\widetilde{\mathbf{U}}(r,n,\xi,\omega)$ and $\widetilde{\mathbf{T}}_r(r,n,\xi,\omega)$. By satisfying compatibility and equilibrium at the soil-tunnel interface and setting the traction field at the tunnel-invert $\widetilde{\mathbf{p}}_{n,ti} = \widetilde{\mathbf{q}}_n$, Eq.(3)-(8) can be rearranged to calculate the vector coefficients:

$$\widetilde{\mathbf{c}} = \left[\begin{array}{c} \left.\widetilde{\mathbf{T}}_r\right|_{r=r_{ti}} \\ \left.\widetilde{\mathbf{T}}_r\right|_{r=r_{to}} - \left.\widetilde{\mathbf{T}}_m\right|_{r=r_{to}} \left.\widetilde{\mathbf{U}}_m^{-1}\right|_{r=r_{to}} \left.\widetilde{\mathbf{U}}\right|_{r=r_{to}} \end{array} \right]^{-1} \left\{ \begin{array}{c} \widetilde{\mathbf{q}}_n \\ \widetilde{\mathbf{p}}_{n,si}^{\mathrm{inc}} - \left.\widetilde{\mathbf{T}}_m\right|_{r=r_{to}} \left.\widetilde{\mathbf{U}}_m^{-1}\right|_{r=r_{to}} \widetilde{\mathbf{u}}_{n,si}^{\mathrm{inc}} \end{array} \right\}, \tag{9}$$

$$\widetilde{\mathbf{b}} = \left.\widetilde{\mathbf{U}}_m^{-1}\right|_{r=r_{to}} \left.\widetilde{\mathbf{U}}\right|_{r=r_{to}} \widetilde{\mathbf{c}}, \tag{10}$$

Substituting Eq.(9)-(10) into Eq.(7)-(8) computes the displacement and traction fields at the soil-tunnel interface of a tunnel excited by the loads represented in Fig. 2. Note that, for the first iteration, $\widetilde{\mathbf{u}}_{n,si}^{\mathrm{inc}} = \widetilde{\mathbf{p}}_{n,si}^{\mathrm{inc}} = \mathbf{0}$ because the free surface has not yet been excited by the tunnel; this is equivalent to the soil response predicted by the PiP model for a full-space [12].

2.2 Step 2: The fictitious-force method for a half-space

In the second calculation step, the incident displacement-field $\mathbf{u}_{fs}^{\mathrm{inc}}$ that propagates towards the free surface from the excited tunnel is calculated using the fictitious-force method. A detailed overview of the fictitious-force method for a tunnel embedded in a homogeneous half-space is provided by Hussein at al. [4].

The fictitious-force method calculates an internal source at the soil-tunnel interface that produces the same displacement field $\widetilde{\mathbf{u}}_{n,si}$ around the tunnel embedded in a full-space. The internal source can be discretised into an equivalent set of M fictitious line-loads $\widetilde{\mathbf{f}}_{(p)}$ in the wavenumber-frequency (ξ,ω)-domain. In the Cartesian coordinate system (x,y,z) shown in Fig. 3, each line-load evaluated at θ_p can be written as

$$\widetilde{\mathbf{f}}_{(p)}(\xi, \omega) = \left\{ \widetilde{f}_x, \widetilde{f}_y, \widetilde{f}_z \right\}^{\mathrm{T}} \quad \text{for } p = 1, 2, \ldots, M \,. \tag{11}$$

The fictitious line-loads are then applied in a half-space, where the tunnel cavity is filled in with soil, as shown in Fig. 3. The line-loads are transformed into the wavenumber-wavenumber-frequency (ξ, γ, ω)-domain by applying the spatial Fourier transform:

$$
\begin{aligned}
\widehat{\mathbf{f}}_{(p)}(\xi, \gamma, \omega) &= \int_{-\infty}^{\infty} \widetilde{\mathbf{f}}_{(p)}(\xi, y, \omega) \cdot e^{-i\gamma y} dy \,, \\
&= \int_{-\infty}^{\infty} \widetilde{\mathbf{f}}_{(p)}(\xi, \omega) \cdot \delta\left(y - r_{to} \sin \theta_p\right) \cdot e^{-i\gamma y} dy \,, \\
&= \widetilde{\mathbf{f}}_{(p)}(\xi, \omega) \cdot e^{-i\gamma r_{to} \sin \theta_p} \,,
\end{aligned}
\tag{12}
$$

where γ is the wavenumber with respect to the coordinate y along the tunnel's transverse axis.

When the fictitious line-loads are expressed as Eq.(12), the Green's functions for a 2.5D elastodynamic half-space [13] are used to find the far-field displacements in the soil. Thus, the incident displacement-field $\widehat{\mathbf{u}}_{fs}^{\mathrm{inc}}$ at the free surface is calculated as a summation of the fictitious line-loads:

$$\widehat{\mathbf{u}}_{fs}^{\mathrm{inc}}(\xi, \gamma, z, \omega) = \sum_{p=1}^{M} \widehat{\mathbf{G}}_{u(p)}^{\mathrm{half}} \, \widehat{\mathbf{f}}_{(p)} \,, \tag{13}$$

where the 3×3 matrix $\widehat{\mathbf{G}}_{u(p)}^{\mathrm{half}}$ contains the 2.5D half-space Green's functions:

$$
\widehat{\mathbf{G}}_{u(p)}^{\mathrm{half}}(\xi, \gamma, \omega) =
\begin{bmatrix}
\widehat{G}_{u_{xx}}^{\mathrm{half}} & \widehat{G}_{u_{xy}}^{\mathrm{half}} & \widehat{G}_{u_{xz}}^{\mathrm{half}} \\
\widehat{G}_{u_{yx}}^{\mathrm{half}} & \widehat{G}_{u_{yy}}^{\mathrm{half}} & \widehat{G}_{u_{yz}}^{\mathrm{half}} \\
\widehat{G}_{u_{zx}}^{\mathrm{half}} & \widehat{G}_{u_{zy}}^{\mathrm{half}} & \widehat{G}_{u_{zz}}^{\mathrm{half}}
\end{bmatrix} \,.
\tag{14}
$$

The spatial Fourier transform can be applied twice to Eq.(13), with respect to the γ and ξ wavenumbers, to evaluate the incident displacement-field at the position $\mathbf{x} = \{x, y, z\}^{\mathrm{T}}$:

$$\mathbf{u}_{fs}^{\mathrm{inc}}(\mathbf{x}, \omega) = \left(\frac{1}{2\pi}\right)^2 \int_{-\infty}^{\infty} \int_{-\infty}^{\infty} \widehat{\mathbf{u}}_{fs}^{\mathrm{inc}}(\xi, \gamma, z, \omega) \cdot e^{i\gamma y} \cdot e^{i\xi x} d\gamma d\xi \,. \tag{15}$$
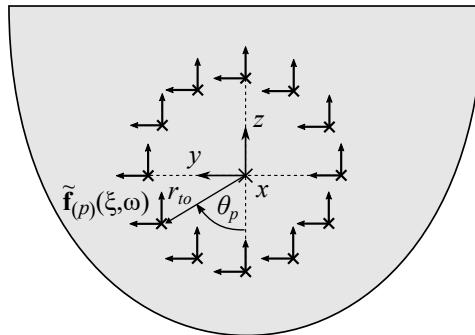

Figure 3: The internal source is represented using an equivalent set of fictitious line-loads at the soil-tunnel interface of a tunnel filled in with soil, where the line-load at θ_p is $\widetilde{\mathbf{f}}_{(p)}(\xi, \omega)$.

2.3 Step 3: The BEM model for internal points

In the third step, the BEM in the space-frequency $(\mathbf{x}, \omega)$-domain is used to calculate the incident-fields that propagate towards the soil-tunnel interface as a result of the tunnel exciting the free surface in the previous step. An unbounded 3D mesh, as shown in Fig. 4, is used to discretise the free surface and the soil-tunnel interface in the soil domain into smooth, constant rectangular elements. The numbers of elements N_1, N_2 and N_x are constrained so that $N_1 = N_2 = N_x$. The elements at the soil-tunnel interface are regarded as internal points within the soil domain, as illustrated by the dashed circle in Fig. 1(c).

By implementing the BEM for internal points in the soil domain, the incident displacement $\mathbf{u}_{si}^{\text{inc}}$ and traction $\mathbf{p}_{si}^{\text{inc}}$ fields at the soil-tunnel interface are calculated using the following matrix equations:

$$\mathbf{u}_{si}^{\text{inc}}(\mathbf{x}, \omega) = \mathbf{G}_u \mathbf{p}_{fs} - \mathbf{H}_u \mathbf{u}_{fs}, \tag{16}$$

$$\mathbf{p}_{si}^{\text{inc}}(\mathbf{x}, \omega) = \mathbf{G}_p \mathbf{p}_{fs} - \mathbf{H}_p \mathbf{u}_{fs}, \tag{17}$$

where the matrices $\mathbf{G}_u$, $\mathbf{H}_u$, $\mathbf{G}_p$ and $\mathbf{H}_p$ contain the full-space Green's functions for the displacements and tractions at internal points [14]. Since the free surface simply responds to the far-field displacements from the tunnel, $\mathbf{u}_{fs} = \mathbf{u}_{fs}^{\text{inc}}$. Note also that $\mathbf{p}_{fs} = \mathbf{0}$ as, by definition, the free surface has zero normal stresses.

In order to apply the incident fields at the soil-tunnel interface as external loads on the tunnel in the next iteration, the incident fields must be transformed from the $(\mathbf{x}, \omega)$-domain into the (n, ξ, ω)-domain. This is achieved by applying the spatial Discrete Fourier Transform with respect to the x coordinate, and by applying a Fourier series expansion in the θ direction around the soil-tunnel interface.
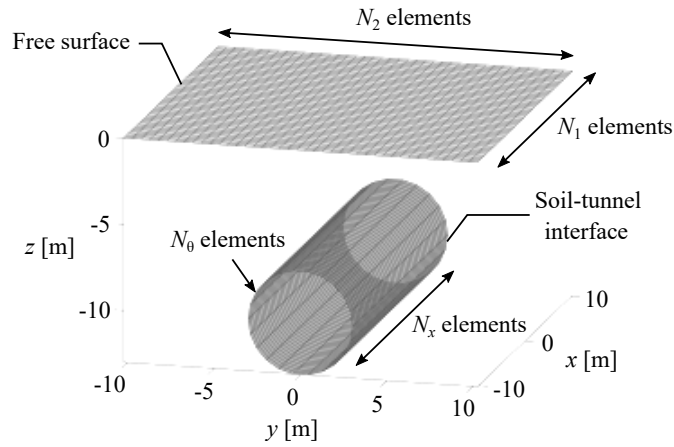

Figure 4: The discretised free surface and soil-tunnel interface (internal points) in the unbounded BEM mesh.

3 Results

In order to verify the proposed method, a number of displacement frequency-response functions (FRFs) are predicted at the free surface using the iterative PiP-BEM model and compared against published results from the 2.5D FEM-BEM model developed by François et al. [8]. The FRFs at the points $(0\,\text{m}, 0\,\text{m}, 0\,\text{m})$ and $(20\,\text{m}, 20\,\text{m}, 0\,\text{m})$ on the free surface are evaluated, as illustrated in Fig. 5. Three different tunnel depths D are also considered: shallow ($5\,\text{m}$), medium depth ($10\,\text{m}$) and deep ($20\,\text{m}$).

For all cases, the tunnel has an inner radius $r_{ti} = 2.75\,\text{m}$ and an outer radius $r_{to} = 3.0\,\text{m}$, and is constructed out of concrete with Young's modulus $E = 50\,\text{GPa}$, Poisson's ratio $\nu = 0.3$ and density $\rho = 2500\,\text{kg/m}^3$. Material damping is introduced through a hysteretic loss factor $\eta = 0.03$ associated with both elastic Lamé

constants. Furthermore, the tunnel is embedded in a homogeneous, isotropic half-space with phase speeds $c_S = 200$ m/s and $c_P = 400$ m/s, for shear and pressure waves, density $\rho = 1800$ kg/m^3 and hysteretic loss factor $\eta = 0.04$ associated with both elastic Lamé constants.
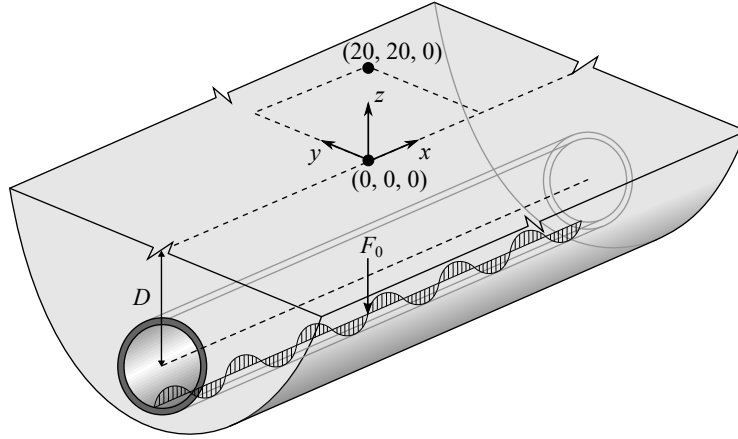

Figure 5: Schematic diagram indicating the two points on the free surface where the displacement FRF is predicted for an underground tunnel excited at the tunnel invert by a vertical, time-harmonic point force F_0.
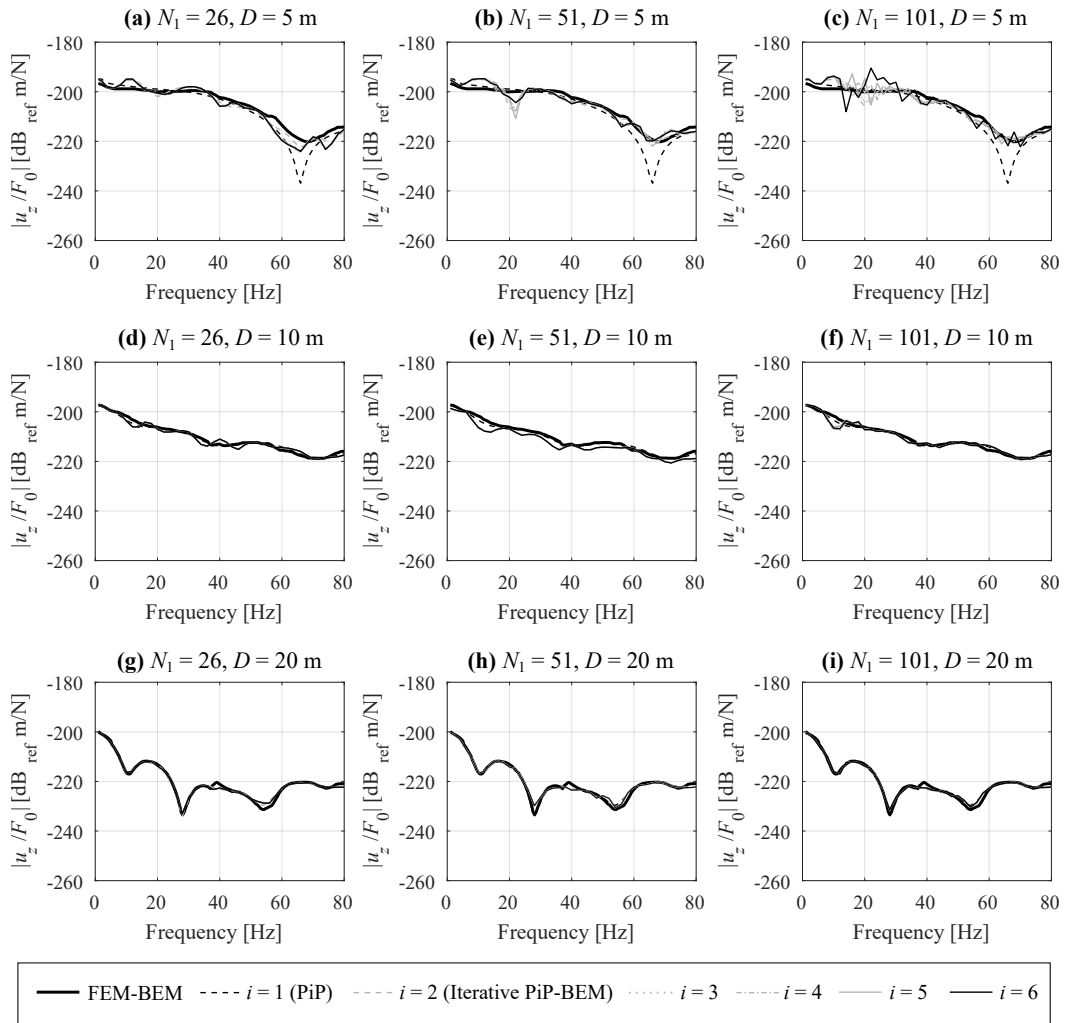

Figure 6: Magnitude of the vertical displacement FRFs at the point $(0 \text{ m}, 0 \text{ m}, 0 \text{ m})$ for different tunnel depths $D = 5 \text{ m}, 10 \text{ m}, 20 \text{ m}$ and number of elements $N_1 = 26, 51, 101$ in the BEM meshes.
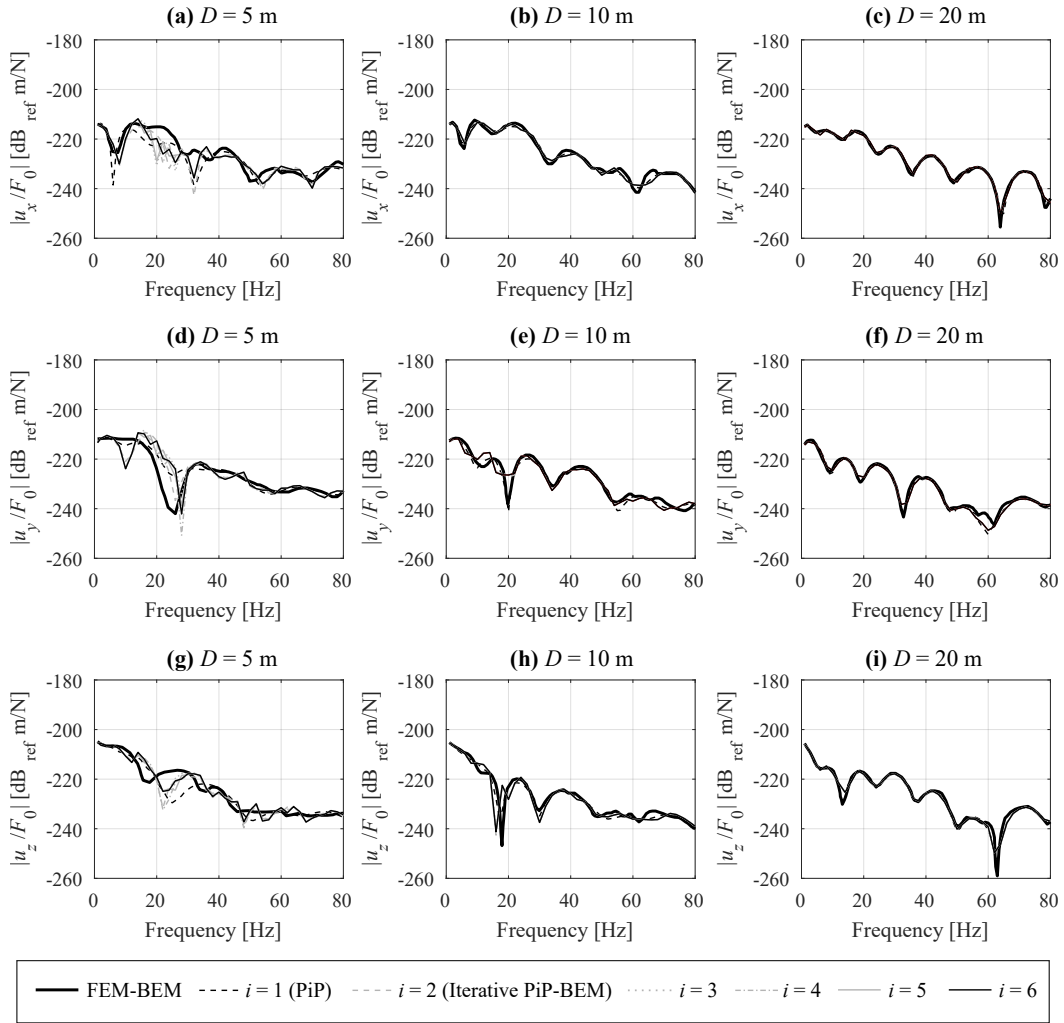
Figure 7: Magnitude of the displacement FRFs in the (a)-(c) longitudinal, (d)-(f) transverse and (g)-(i) vertical directions at the point $(20\,\text{m}, 20\,\text{m}, 0\,\text{m})$ for different tunnel depths $D = 5\,\text{m}, 10\,\text{m}, 20\,\text{m}$.

In the BEM mesh, the size of the elements at the free surface and soil-tunnel interface are $0.4\,\text{m} \times 0.4\,\text{m}$ and $0.4\,\text{m} \times 0.448\,\text{m}$, respectively. This ensures that there are at least six elements per wavelength, as recommended by Domínguez [15], over the frequency range of 1–80 Hz.

Figure 6 plots the vertical displacement FRFs at the point $(0\,\text{m}, 0\,\text{m}, 0\,\text{m})$, directly above the excitation point, using up to six iterations of the PiP-BEM model over the frequency range of interest. For a tunnel depth $D \geq 10\,\text{m}$, there is good agreement between the PiP-BEM model and the FEM-BEM model over the full frequency range, and the FRFs have converged after just one iteration ($i = 1$). This is expected because the tunnel is located far from the free surface. Note that, for the first iteration, the FRFs are directly equivalent to those predicted by the half-space PiP model.

For a shallow tunnel, with $D = 5\,\text{m}$, there is a greater difference between the first iteration ($i = 1$) of the PiP-BEM model and the FEM-BEM model, particularly at high frequencies (above approximately 60 Hz). There is a clear anti-resonance trough in the FRF of the first iteration at $\approx 64\,\text{Hz}$, which corresponds to a shear wavelength of $\lambda_S \approx 3.1\,\text{m}$ in the soil. In general, anti-resonances of a system can be interpreted as the resonances of the system when fixed at the excitation point [16]. At 64 Hz, the distance between the tunnel-invert, where the point force is applied, and the free surface at $(0\,\text{m}, 0\,\text{m}, 0\,\text{m})$ is ≈ 2.5 shear wavelengths. Thus, the anti-resonance is consistent with the destructive interference caused by shear waves when the presence of the tunnel is neglected in the soil sub-system, i.e. when applying the fictitious-force method. This anti-resonance is not present when using either the FEM-BEM model or when more iterations are ap-

plied using the proposed method. It is clear that the iterative PiP-BEM model captures the coupled response of the soil-tunnel system by allowing the free surface to influence the tunnel's response and eliminating the destructive interference caused by shear waves.

Figure 6 also shows that, as the number of elements used in the BEM mesh is increased from $N_1 = 26$ to $N_1 = 51$ for a tunnel with $D = 5$ m, the agreement between the proposed method and the FEM-BEM model improves. This is expected because a greater extent of the free-surface and soil-tunnel interface is discretised in the BEM mesh, which prevents waves from leaking around the edges of the mesh. However, when the number of elements is increased from $N_1 = 51$ to $N_1 = 101$, fluctuating artefacts appear in the FRF. The most likely explanation for this phenomenon is that the distance between the soil-tunnel interface and free surface is very close over a large extent of the BEM mesh for a shallow tunnel. Therefore, the unbounded mesh closely resembles a bounded mesh; this can cause the integral equations in the BEM to lose the uniqueness of solutions at certain frequencies, known as fictitious eigenfrequencies [15]. Typically, the use of full-space Green's functions with an appropriately discretised boundary does not result in fictitious eigenfrequencies [17].

Figure 7 plots the longitudinal, transverse and vertical displacement FRFs at the point $(20 \text{ m}, 20 \text{ m}, 0 \text{ m})$, again using the first six iterations of the PiP-BEM model. To minimise the fluctuating artefacts in the FRFs, $N_1 = 51$ elements are used in the BEM mesh. Again, there is good agreement between the proposed method and the FEM-BEM model when $D \geq 10$ m. For a shallow tunnel, the FRFs predicted by the iterative PiP-BEM model agree better with those predicted by the FEM-BEM model, when compared to the PiP model for a half-space.

4 Conclusions

This study demonstrates that the iterative PiP-BEM model agrees well with the coupled FEM-BEM model for predicting the soil response around a tunnel embedded in a homogeneous half-space over the typical frequency range (1–80 Hz) associated with ground-borne vibration. Compared to the half-space PiP model, the iterative wave-scattering approach introduced in this paper better captures the coupled response of shallow tunnels by accounting for the scattered-fields at both the free surface and the soil-tunnel interface. As a general rule, a good solution is obtained using the half-space PiP model if the distance between the tunnel and the free surface is larger than the tunnel diameter.

Future work will involve coupling a railway train-track system to the tunnel-invert in the iterative PiP-BEM model and to investigate numerical schemes that will minimise the fluctuating artefacts in the FRFs. In addition, the BEM in this paper uses the 3D Green's functions for a full-space because the railway tunnel will eventually be coupled to a BEM model for a 3D pile-group, which will be the subject of a future paper on the train-induced response of pile foundations.

Acknowledgements

References

[1] M. F. M. Hussein and H. E. M. Hunt. *PiP: A software for calculating vibration from underground railways.* http://pipmodel.eng.cam.ac.uk/PiP.html. (accessed June, 15 2020).

[2] H. E. M. Hunt, M. F. M. Hussein, and W. I. Hamad. "The PiP model and progress in ground vibration from railways". In: *Proceedings of the Annual Conference of the Australian Acoustical Society*. Perth, Australia, 2017, pp. 1–9.

[3] M. F. M. Hussein and H. E. M. Hunt. "A numerical model for calculating vibration from a railway tunnel embedded in a full-space". In: *Journal of Sound and Vibration* 305.3 (2007), pp. 401–431. DOI: 10.1016/j.jsv.2007.03.068.

[4] M. F. M. Hussein, S. Gupta, H. E. M. Hunt, et al. "An efficient model for calculating vibration from a railway tunnel buried in a half-space". In: *Proceedings of the 13th International Congress on Sound and Vibration*. Vienna, Austria, 2006.

[5] M. F. M. Hussein, H. E. M. Hunt, L. Rikse, et al. "Using the PiP model for fast calculation of vibration from a railway tunnel in a multi-layered half-space". In: *Proceedings of the 9th International Workshop on Railway Noise*. Munich, Germany, 2008, pp. 136–142. DOI: 10.1007/978-3-540-74893-9.

[6] S. Gupta, M. F. M. Hussein, G. Degrande, et al. "A comparison of two numerical models for the prediction of vibrations from underground railway traffic". In: *Soil Dynamics and Earthquake Engineering* 27.7 (2007), pp. 608–624. DOI: 10.1016/j.soildyn.2006.12.007.

[7] M. F. M. Hussein, S. François, M. Schevenels, et al. "The fictitious force method for efficient calculation of vibration from a tunnel embedded in a multi-layered half-space". In: *Journal of Sound and Vibration* 333.25 (2014), pp. 6996–7018. DOI: 10.1016/j.jsv.2014.07.020.

[8] S. François, M. Schevenels, P. Galvín, et al. "A 2.5D coupled FE–BE methodology for the dynamic interaction between longitudinally invariant structures and a layered halfspace". In: *Computer Methods in Applied Mechanics and Engineering* 199.23-24 (2010), pp. 1536–1548. DOI: 10.1016/J.CMA.2010.01.001.

[9] X. Li and J. A. Hudson. "Multiple scattering of elastic waves from a continuous and heterogeneous region". In: *Geophysical Journal International* 126 (1996), pp. 845–862. DOI: 10.1111/j.1365-246X.1996.tb04707.x.

[10] T. E. Doyle. "Iterative simulation of elastic wave scattering in arbitrary dispersions of spherical particles". In: *The Journal of the Acoustical Society of America* 119 (2006), pp. 2599–2610. DOI: 10.1121/1.2184989.

[11] MathWorks Ltd. MATLAB, Version 9.7, R2019b, Cambridge, U.K., 2019.

[12] J. A. Forrest and H. E. M. Hugh. "A three-dimensional tunnel model for calculation of train-induced ground vibration". In: *Journal of Sound and Vibration* 294.4-5 (2006), pp. 678–705. DOI: 10.1016/j.jsv.2005.12.032.

[13] A. J. B. Tadeu, J. António, and L. Godinho. "Green's function for two-and-a-half dimensional elastodynamic problems in a half-space". In: *Computational Mechanics* 27.6 (2001), pp. 484–491. DOI: 10.1007/s004660100259.

[14] J. J. Rego Silva, H. Power, and L. C. Wrobel. "A boundary element method for 3D time-harmonic elastodynamics - Numerical aspects". In: *Boundary Elements XV Vol 2 Stress Analysis*. WIT Press, 1993, pp. 423–439.

[15] J. Domínguez. *Boundary Elements in Dynamics*. Southampton & Essex, UK: Computational Mechanics Publications & Elsevier Applied Science, 1993.

[16] F Wahl, G Schmidt, and L Forrai. "On the significance of antiresonance frequencies in experimental structural analysis". In: *Journal of Sound and Vibration* 219.3 (1999), pp. 379–394. DOI: 10.1006/jsvi.1998.1831.

[17] D. E. Beskos. "Wave propagation through ground". In: *Boundary Element Techniques in Geomechanics*. Ed. by G D Manolis and T G Davies. Computational Mechanics Publications & Elsevier Applied Science, 1993. Chap. 11, pp. 359–406.